LOFAR detectability of prompt low-frequency radio emission during gamma-ray burst X-ray flares

Starling, R.L.C.; Rowlinson, A.; van der Horst, A.J.; Wijers, R.A.M.J.

DOI
10.1093/mnras/staa1168

Publication date
2020

Document Version
Final published version

Published in
Monthly Notices of the Royal Astronomical Society

Monthly Notices
of the
ROYAL ASTRONOMICAL SOCIETY

MNRAS **494,** 5787–5792 (2020)
Advance Access publication 2020 April 30

doi:10.1093/mnras/staa1168

LOFAR detectability of prompt low-frequency radio emission during gamma-ray burst X-ray flares

R. L. C. Starling [1★†] A. Rowlinson [2,3] A. J. van der Horst[4,5] and R. A. M. J. Wijers [3]

[1]*School of Physics and Astronomy, University of Leicester, University Road, Leicester LE1 7RH, UK*
[2]*Netherlands Institute for Radio Astronomy (ASTRON), PO Box 2, NL-7990 AA Dwingeloo, the Netherlands*
[3]*Anton Pannekoek Institute, University of Amsterdam, Postbus 94249, NL-1090 GE Amsterdam, the Netherlands*
[4]*Department of Physics, The George Washington University, 725 21st St NW, Washington, DC 20052, USA*
[5]*Astronomy, Physics and Statistics Institute of Sciences (APSIS), The George Washington University, Washington, DC 20052, USA*

Accepted 2020 April 22. Received 2020 April 22; in original form 2020 April 5

ABSTRACT

The prompt emission in long gamma-ray bursts (GRBs) arises from within relativistic outflows created during the collapse of massive stars, and the mechanism by which radiation is produced may be either magnetically or matter dominated. In this work, we suggest an observational test of a magnetically dominated Poynting flux model that predicts both γ-ray and low-frequency radio pulses. A common feature among early light curves of long GRBs are X-ray flares, which have been shown to arise from sites internal to the jet. Ascribing these events to the prompt emission, we take an established *Swift* XRT flare sample and apply a magnetically dominated wind model to make predictions for the timing and flux density of corresponding radio pulses in the ∼100–200 MHz band observable with radio facilities such as LOFAR. We find that 44 per cent of the X-ray flares studied would have had detectable radio emission under this model, for typical sensitivities reached using LOFAR's rapid response mode and assuming negligible absorption and scattering effects in the interstellar and intergalactic medium. We estimate the rate of *Swift* GRBs displaying X-ray flares with detectable radio pulses, accessible to LOFAR, of order seven per year. We determine that LOFAR triggered observations can play a key role in establishing the long debated mechanism responsible for GRB prompt emission.

Key words: gamma-ray burst: general – radio continuum: transients – X-rays: bursts.

1 INTRODUCTION

Gamma-ray bursts (GRBs) show a rich diversity in their temporal behaviour, particularly in the early stages of their evolution. The prompt emission is usually recorded by γ-ray instruments operating at energies above ∼10 keV, and consists of one or more pulses with varying peak fluxes, widths, and separations. The prompt γ-ray emission may arise from either a matter dominated, hydrodynamical flow dissipating energy at shock fronts (e.g. Rees & Mészáros 1994), or from a magnetically dominated outflow in which energy dissipation can occur via magnetic reconnection (e.g. Spruit, Daigne & Drenkhahn 2001; Sironi, Petropoulou & Giannios 2015). Whether the prompt emission arises from a matter-dominated or magnetically dominated outflow remains a central outstanding question in GRB physics.

Following the prompt γ-ray emission, longer wavelength observations are possible after a spacecraft slew; the *Neil Gehrels Swift Observatory* (hereafter *Swift*; Gehrels et al. 2004) has a typical prompt slew time of just 100 s. Some X-ray observations show a continuation of the pulse-like behaviour of the central engine, before transitioning through a steep temporal decay phase to a power-law afterglow understood to be the product of synchrotron radiation (e.g. Sari, Piran & Narayan 1998). Superposed on the smooth power-law decay light curve, late-time pulse-like features can be seen, termed flares. Flares have been detected across the wavelength range from X-rays, through optical, down to radio, but are most common in the X-ray band possibly due to the impressive coverage of GRB X-ray light curves with *Swift*.

Swift is a GRB-dedicated facility, triggering on 15–350 keV γ-rays with the Burst Alert Telescope (BAT; Barthelmy et al. 2005) and rapidly following up in the 0.3–10 keV band with the X-Ray Telescope (XRT; Burrows et al. 2005), and in multiple bands spanning 170–650 nm with the UV and Optical Telescope (UVOT; Roming et al. 2005). Among all BAT-triggered GRBs, the XRT detects ∼ 95 per cent (Evans et al. 2009), of which about half

★ E-mail: rlcs1@le.ac.uk
† ASTRON Helena Kluyver Visiting Fellow.

display X-ray flaring activity (48 per cent, Swenson & Roming 2014). In a handful of cases, optical flares are seen during high-energy flaring periods (e.g. Cucchiara et al. 2011; Martin-Carrillo et al. 2014; Vestrand et al. 2014; Troja et al. 2017, note that observational coverage is one factor here). The sharp optical peaks are often attributed to a reverse shock–forward shock combination, according to the standard fireball model (Sari & Piran 1999).

An internal origin for X-ray flares has long been favoured (e.g. Chincarini et al. 2007; Falcone et al. 2007; Chincarini et al. 2010; Bernadini et al. 2011), based on the similarity of their temporal properties to prompt GRB pulses, including relative rise time, duration and decay time, and distribution of waiting times (Guidorzi et al. 2015). Both X-ray flares and prompt pulses show a wide variation in both time since trigger and peak flux, and an increased width and decreased peak flux for later time flares (e.g. Guidorzi et al. 2015).

A connection with the prompt emission is also evident from coincident X-ray flare activity and tens to hundreds of keV γ-ray pulses (demonstrated in e.g. Hu et al. 2014; Oganesyan et al. 2018, currently limited to a small number of GRBs since instrumental coverage in γ-rays and X-rays must overlap). A 3 yr study using data from *Swift* and *Fermi* (Meegan et al. 2009) concluded that X-ray flares can be produced via the late internal shock model of prompt emission, and therefore can be effective probes of the central engine and its activity (Troja et al. 2015, as could the rarer prompt optical flares, see e.g. Troja et al. 2017). A single power law is an acceptable fit to ∼80 per cent of the X-ray spectra of *Swift* GRBs for which BAT and XRT coverage overlaps (Evans et al. 2010). Band (Band, Matteson & Ford 1993), band-cut (Zheng et al. 2012), and cut-off power-law models are often a better description of spectra across the γ-ray band. Simultaneous *Fermi* GBM, *Swift* BAT, and XRT spectral fits have shown that in 62 per cent of cases extending these models down to X-ray energies results in a further, low energy break with spectral indices consistent with a single, broad-band synchrotron component in the fast cooling regime (Oganesyan et al. 2018, but see also Guiriec et al. 2016).

Wang & Dai (2013) and Yi et al. (2016) compared GRB flare properties with those of Solar flares and concluded that they are strikingly similar. This motivates the investigation of magnetically dominated models for the production of X-ray flares and indeed GRB prompt emission (e.g. Smolsky & Usov 2000; Uhm & Zhang 2016b), while matter-dominated models also remain viable (e.g. Rees & Mészáros 1994, 2005). Some studies of *Swift* X-ray flares that consider the steeply decaying segment as arising from off-axis jet angles, referred to as high latitude emission or the curvature effect, have concluded that the emitting region must be undergoing bulk acceleration, requiring additional energy supplied by a significant Poynting flux component (Jia, Uhm & Zhang 2016; Uhm & Zhang 2016a). Given these connections between X-ray and γ-ray pulses, and some evidence for a magnetically powered component, we might reasonably expect to apply prompt emission models also to X-ray flares. For instance the magnetically driven wind model proposed by Usov & Katz (2000) includes the generation of early radio emission peaking at low frequencies. Probing GRB prompt emission mechanisms through X-ray flares has the advantage that flaring begins with or after the γ-ray pulses, and can continue for a significant fraction of both prompt and afterglow phases relaxing the requirements on telescope response times.

Radio observations have traditionally begun hours to weeks after the GRB, as this is when a radio afterglow, caused by interaction of the forward shock with the circumburst medium, is expected (e.g. Katz 1994; Chandra & Frail 2012; Anderson et al. 2018a). Prompt searches for radio emission have also been carried out, constraining prompt radio emission to lie below several thousand Janskys (e.g. Dessenne et al. 1996; Balsano et al. 1998). Alas this is too insensitive to probe many of the proposed prompt radio emission mechanisms. Recent studies have focused on searching for fast radio bursts at GHz frequencies in the first few minutes of a GRB, associated with the plateau phases (Bannister et al. 2012), or a deeper search, ∼ Jy sensitivity, for prompt (minute to hours) radio emission from short GRBs (Kaplan et al. 2016; Anderson et al. 2018b). This was followed by a catalogue of <1 d follow-up observations at 15.7 GHz with the Arcminute Microkelvin Imager which increased the number of radio detections of short and long GRBs (Staley et al. 2013; Anderson et al. 2018a). The new detections spanned 0.3–33 d post-burst, meaning that coverage during the prompt emission itself remains largely unexplored.

Recently, a rapid response mode was implemented for the LOw Frequency ARray (LOFAR; Van Haarlem et al. 2013). LOFAR operates using either its low band antenna (LBA, 10–90 MHz) or with its high band antenna (HBA, 120–240 MHz) and is capable of responding to transient alerts within 5 min of receiving the trigger notice. Rowlinson et al. (2019) outline the first LOFAR search for prompt radio emission in long GRB 180706A, beginning 4.5 min after the γ-ray trigger. By utilizing the full capability of LOFAR, the observational constraints for coherent radio emission can now reach mJy sensitivities, revolutionizing the search for this emission from many transient events.

In this paper, we explore the detectability of low-frequency radio waves associated with X-ray flares, under the assumptions of a Poynting flux model for the prompt emission mechanism in which X-ray flares are a manifestation of prompt non-thermal pulses. We draw a subset of X-ray flares from an established sample, and apply the model to estimate the fraction of low-frequency waves that would have been detectable by LOFAR for a given set of observational conditions. We discuss the optimal strategy to apply to the current LOFAR triggering and data processing, to find the emission from flares expected within this framework.

2 MODEL

Low-frequency waves have been postulated to arise at the shock front of a highly magnetized, relativistic wind (generated by the rotational energy of a compact object) interacting with its surroundings (Smolsky & Usov 2000; Usov & Katz 2000). In this model, a variable current flowing between the two media either side of the travelling shock front leads to the generation of low-frequency radio waves in the MHz regime.

The radio emission should occur at a peak frequency, $\nu_{\rm max}$, in the observed frame of

$$\nu_{\rm max} = \frac{1}{1+z}\frac{B_0}{10^2}\ {\rm MHz}, \tag{1}$$

where z is the redshift of the GRB and we adopt an observer frame value of $B_0 = 10^2\epsilon_B^{1/2}$ G for the magnetic field in the wind at the radius of low-frequency wave generation (Usov & Katz 2000), where ϵ_B is the fraction of the total energy in the magnetic field. We note there are several assumptions embedded within equation (1), such as the properties of the magnetic wind and the deceleration radius (see Usov & Katz 2000, for further details regarding these assumptions).

A delay is expected between the emission of the radio pulse and observation, due to dispersion along the line of sight, of

$$\tau(\nu) \sim \frac{\rm DM}{241\ \nu^2}\ {\rm s} \tag{2}$$

in the observer frame, where ν is the observer frequency in GHz (Taylor & Cordes 1993). The dispersion measure, DM $= \int n_e D_L$ pc cm^{-2}, can be estimated using the relation derived from intergalactic medium modelling: DM $\sim 1200z$ (e.g. Ioka 2003; Inoue 2004; Lorimer et al. 2007).

The observed duration of the pulse, τ_r, is

$$\tau_r(\nu, \Delta\nu) \sim 2\frac{\Delta\nu}{\nu}\tau(\nu)\ \mathrm{s}, \quad (3)$$

(Usov & Katz 2000) where $\Delta\nu$ is the bandwidth and $\tau(\nu)$ is the dispersion-induced signal delay in seconds.

Following Usov & Katz (2000), we calculate the expected flux density in the MHz bands by assuming a ratio, δ, between fluence spectral densities in radio and in γ-rays. In the two regimes of non-dispersion-limited and dispersion-limited, the predicted radio flux density, F_ν, is

$$F_\nu = \begin{cases} \dfrac{\delta(\beta-1)}{\tau_r \nu_{\max}}\left(\dfrac{\nu}{\nu_{\max}}\right)^{-\beta}\dfrac{\Phi_\gamma}{10^{-23}}\ \mathrm{Jy}, & \tau_r \le \dfrac{2\Delta\nu}{\nu}\tau(\nu) \\ \dfrac{\delta(\beta-1)}{2\Delta\nu\tau}\left(\dfrac{\nu}{\nu_{\max}}\right)^{1-\beta}\dfrac{\Phi_\gamma}{10^{-23}}\ \mathrm{Jy}, & \tau_r > \dfrac{2\Delta\nu}{\nu}\tau(\nu) \end{cases}, \quad (4)$$

where $\delta \sim 0.1\epsilon_B$, β is the power-law spectral slope in the high-frequency tail typically assumed to be 1.6, τ_r is the intrinsic duration of the radio pulse (s), $\Delta\nu$ is the bandwidth (Hz), $\tau(\nu)$ is the dispersion-induced signal delay (s) and Φ_γ is the bolometric γ-ray fluence spectral density (erg cm^{-2}). The fraction of energy in the magnetic field $\epsilon_B = 10^{-3}$ is adopted following the limits given in Katz (1997).

Assuming that the radio pulse has the same duration as the X-ray pulse, we determine within which of the two regimes each X-ray flare occurs. The appropriate form of equation (4) can then be applied.

The flux density predictions are made for each X-ray flare individually using the above equations. Multiple flares may well occur in an observation window and in that case we could input their combined fluence here in the way that the model is utilized for prompt emission inputs in Usov & Katz (2000).

We note that these predictions are dependent upon the low-frequency radio emission being able to propagate freely through the ambient medium of the GRB, the interstellar medium in the host galaxy and the intergalactic medium. Absorption and scattering effects may lead to reduced observable flux densities (for further discussion of these propagation effects, see Rowlinson & Anderson 2019, and references therein).

3 X-RAY FLARE SAMPLE

We adopt the X-ray flare sample of Yi et al. (2016), who identified 468 flares occurring during 10 yr of *Swift* operations up to 2015 March, and fitted their temporal evolution using a smoothly broken power law. Requiring a known redshift, we cut their sample to 200 flares across 81 different GRBs spanning $0.257 < z < 8.23$. Most of our final sample are long GRBs. Two sources have $T_{90} \le 2$ s (GRBs 070724, 131004); flare parameters are observed to be similar for both short and long GRBs (e.g. Margutti et al. 2011) so, despite the very different progenitors that are inferred, the prompt emission mechanisms may be the same and hence we keep these in our selection. Four sources have no T_{90} measurement but on inspection these appear to represent the potential new category of ultralong GRBs for which the emission continues into orbit gaps and can only be estimated as a lower limit (GRBs 111209A, 121027A, 121229A, and 130925; Evans et al. 2014; Levan et al. 2014). The ultralong GRBs are particularly interesting given the higher fraction of prompt emission occurring after XRT slew and ground-based response times compared with classical GRBs.

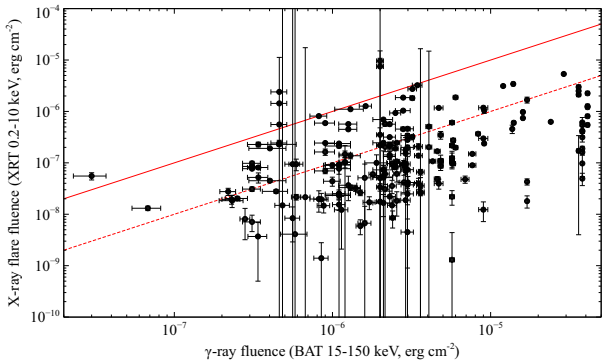

Figure 1. Comparison of the γ-ray fluence integrated over all observed pulses with the X-ray fluences of individual flares. Errors are 90 per cent confidence. For reference, red lines indicate the equality line (solid) and 10 per cent fraction (dashed).

The mean observation start time for XRT following a slew is 113.2 s for this GRB sample and spans 43.9–577.5 s. If the X-ray flare peaks before the spacecraft slew, it cannot be identified as such, and we note that this introduces a bias in the times we adopt for this study of radio pulses. Our minimum observed (rest frame) flare peak time is 59.7 s (13.1 s), with a sample mean of 9760 s (5206 s).

The fluence in X-ray flares might be expected to be of order 10 per cent of the γ-ray fluence (e.g. Chincarini et al. 2010), but rather than making this assumption we use measured X-ray fluences from Yi et al. (2016). We compare these with the measured γ-ray fluences from the Third Swift BAT Catalog (Lien et al. 2016) in Fig. 1.[1] We find that the weighted mean fluence ratio of each individual X-ray flare to the total of its GRB in γ-rays is 0.9 ± 0.1 per cent for this sample. However, the fluence ratio spans a huge range, from 0.02 to 520 per cent (three GRBs have flares whose X-ray fluence exceeds the total measurable γ-ray fluence: 060124, 070724A, and 121027A), and hence we utilize the high-energy fluence for each flare individually in our radio flux density predictions.

4 RESULTS

Taking the sample of X-ray flares as defined in Section 3, we can predict the flux density of the radio flare using equation (4) assuming that we trigger a rapid response observation by LOFAR. This method is also directly applicable to observations with other radio facilities, but LOFAR combines both a sufficiently rapid response mode and the deep observational sensitivity required to test this model.

We find the delay time with respect to the X-ray pulse, τ, and duration of the radio flare, τ_r, predicted for each of the X-ray flares in our sample, and plot their distributions in Fig. 2. We find mean observed (rest frame) values of $t_{\mathrm{flarestart}} + \tau = 8758$ (4630) s and $\tau_r = 15523$ (7745) s. The sample peak frequencies are $0.003 < \nu_{\max} < 0.03$ MHz (using equation 1), so currently detectable fluxes will arise from the high-frequency spectral tail.

[1] https://swift.gsfc.nasa.gov/archive/grb_table/

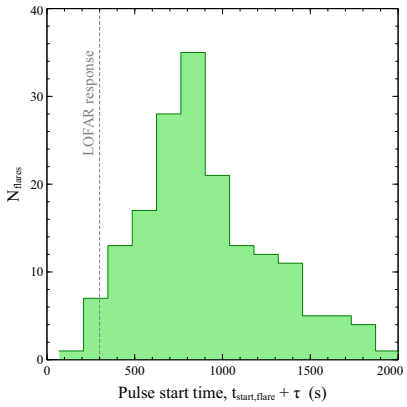

Figure 2. Distribution of expected start times of the radio pulses that occur up to 2000 s. The current LOFAR response time of 5 min is indicated. We note there is a long, low tail to late times but have excluded this here for clarity.

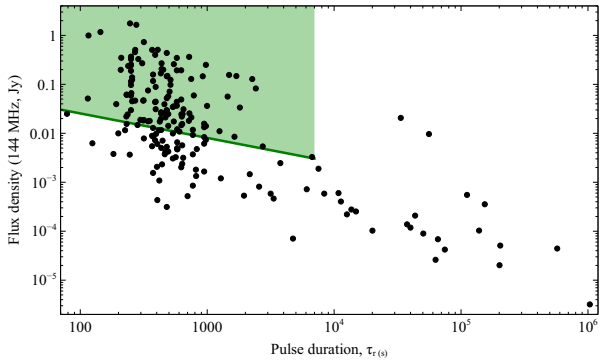

Figure 3. Expectations for flux density at 144 MHz and pulse duration (observer frame). The shaded region indicates detections at or above a 3σ level of duration 2 h or less, based on the sensitivity derived using the rms noise parameters of GRB 180706 (equation 5).

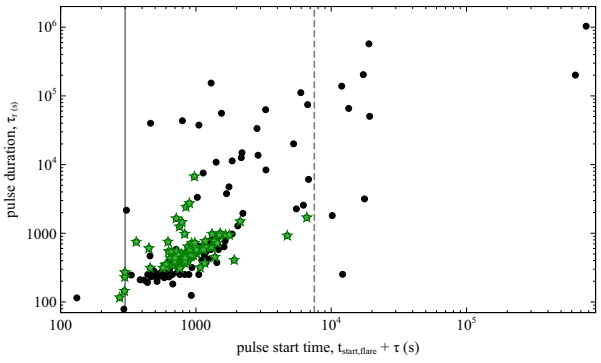

Figure 4. Pulse duration against pulse start time (observer frame). Green stars indicate the flares identified as detectable . The grey line indicates the current LOFAR response time, and the grey dashed line indicates 2 h later, representing a typical integration.

We calculate the expected flux density in a typical LOFAR HBA GRB observation, following the instrumental setup currently used for rapid response mode LOFAR follow-up of GRBs ($\nu = 144$ MHz, $\Delta\nu = 48$ MHz, Rowlinson et al. 2019). The results are plotted in Fig. 3.

We can use the triggered observations of GRB 180706A to quantify the expected sensitivity of future LOFAR observations that are triggered on GRBs containing X-ray flares. The 2 h integrated image of the field of GRB 180706A had an RMS noise of 0.6 mJy beam^{-1} at the location of the GRB, corresponding to a sensitivity of 3 mJy assuming a 5σ detection threshold. Although it is not possible to predict the X-ray flares in advance and hence adapt triggering criteria, we are able to tailor our processing of the radio observations to target the flare specifically following the trigger. For instance, a radio flare that is 5 min long may be undetectable in a 2 h integrated image so instead we can produce 5 min snapshot images in which the background is greatly reduced for shorter pulses (see e.g. Carbone et al. 2017; Rowlinson et al. 2019). Using the general correlation between the sensitivity of a radio image and the integration time ($S \propto t_{\rm int}^{-\frac{1}{2}}$, where S is the detectable flux density in the image and $t_{\rm int}$ is the image integration time in seconds), we extrapolate from the 2 h image properties to estimate the detection threshold in shorter duration snapshot images using

$$S = 3\ \mathrm{mJy} \left(\frac{t_{\rm int}}{7200\ \mathrm{s}}\right)^{-\frac{1}{2}}. \quad (5)$$

A total of 86 flares starting after the 5 min LOFAR response time met the sensitivity criterion of equation (5). This reduces to 85 (42 per cent) of the 200 flares in our sample, when also requiring a start time within the 2 h integration window. The detectable parameter space is indicated as a shaded region in Fig. 3. These 85 flares are spread among 45 individual GRBs. This calculation assumes no significant confusion noise, appropriate for the poorer uv coverage at the time-scales we are investigating.

The flares have a range of durations, τ_r, and delays, τ, from the start of the observation (Fig. 4). We need to determine whether the flares in Fig. 3 are detectable for a given trigger observation, and for this we will work under the assumption that flares have a constant flux density top-hat structure. The telescope has a response time, $T_{\rm resp}$, to transient events and for LOFAR the guaranteed response time is 5 min. Then the observation has a given duration, $T_{\rm dur}$, which we take to be 2 h in this analysis. This leads to two scenarios:

(i) $\tau + \tau_r \leq T_{\rm resp} + T_{\rm dur}$: in which the end of the predicted radio pulse is shorter than the duration of the observation. The detectability of the radio pulse is then determined by its duration, its flux density and the sensitivity of the telescope for the duration of the pulse (as in Fig. 3).

(ii) $\tau + \tau_r > T_{\rm resp} + T_{\rm dur}$: in this case, the radio pulse is much longer than the observation. Therefore, we need to determine if the pulse would be detectable during the telescope observation window. The observable duration, $T_{\rm obs}$, is given by $T_{\rm obs} = \tau_r - [(\tau + \tau_r) - (T_{\rm resp} + T_{\rm dur})]$. We can then predict the sensitivity of the radio observation for an integration time equal to $T_{\rm obs}$ (using equation 5). If the predicted flux density of the radio flare is greater than the expected sensitivity in the image, then the radio flare is detectable.

Performing this calculation, we find 3 flares among the detected subset with stop times after the observation is complete, and of these, two remain detectable. We can apply the same logic to flares beginning before the 5 min response time but with durations that fall inside the observing window. There are 6 of these flares, among which 4 would be detectable.

The resulting proportion of this X-ray flare sample detectable by LOFAR in rapid response mode is 44 per cent, shown as green stars in Fig. 4.

5 DISCUSSION

5.1 Summary of results

We find that a significant fraction, 44 per cent, of X-ray flares should be detectable at low frequencies with current LOFAR instrumentation, if the prompt emission is produced via magnetically dominated processes as described in Usov & Katz (2000). This is very promising for observational searches. Predictions for observing radio flares from short GRBs have been examined using this same model, focusing on the prompt γ-ray flares, and have been shown to be observable with the fastest response radio facilities (Rowlinson & Anderson 2019).

5.2 X-ray flares as prompt emission

We present evidence in Section 1 for the connection between prompt γ-ray pulses and X-ray flares, which is a premise of this analysis, and we now examine this for our sample of flares in particular. Among our 200-strong flare sample, 71 may have started whilst the prompt γ-ray emission was ongoing, since the flare start time lies within the GRB duration according to BAT T_{90}. On the other hand, some flares are really late even in the rest frame and, while it is difficult to assign these to the same internal mechanism at least one late flare study showed that flares occurring $>10^4$ s after trigger (observed frame), generally have the same properties as the larger early flare sample (Curran et al. 2008). These very late flares cannot be probed with 2 h integration times however, so would not be targeted for LOFAR observations.

Oganesyan et al. (2018) studied GRBs with overlapping *Swift* BAT-XRT coverage and fitted their time-averaged joint spectra, including also *Fermi* GBM data where possible. Their sample spans the time frame of the Yi et al. (2016) flare sample, and includes 15 of the GRBs considered in this work (all long, 5 with GBM data). Their results showed that 11 are best fitted with a band or band-cut function, with a low energy break in the XRT band, 1 with a cut-off power law, and 3 sources can be described by a single power law. They apply an offset correction factor between instruments, but in no cases were these too large to accommodate a single origin for the X-ray to γ-ray emission. Oganesyan et al. (2018) argue that even when a low energy break is required, the spectrum can be considered a single, prompt synchrotron component in a fast-cooling regime.

5.3 LOFAR rate predictions

We note that this flare sample probes only a fraction of the total GRB sample which could be accessed by rapid response triggered observations, since it has been limited to known redshift sources (this information usually becomes available only at later times). We therefore estimate the rate of detectable flares with LOFAR, $R_{\rm LOFAR}$, starting from the *Swift* GRB rate of $R_{\rm GRBs}$ of 88.7 yr^{-1} (averaged over 2005–2019),

$$R_{\rm LOFAR} = R_{\rm GRBs} \times f_{\rm XRT} \times f_{\rm flare} \times f_{\rm sky} \times f_{\rm detec} = 7.1\ {\rm yr}^{-1}, \quad (6)$$

where the fraction of GRBs detected with XRT, $f_{\rm XRT}$, is 95 per cent (Evans et al. 2009), the fraction of GRBs with X-ray flares, $f_{\rm flare}$, is taken as 48 per cent (Swenson & Roming 2014), the detectable fraction to LOFAR in rapid response mode at 144 MHz, $f_{\rm detec}$, is 44 per cent from this work, and assuming 40 per cent sky coverage, $f_{\rm sky}$. Just over 20 per cent of LOFAR-accessible GRBs are expected to have an X-ray flare that would be detectable at $\geq 5\sigma$. This can be optimized given the direct correspondence in the adopted model between γ-ray fluence and radio flux density. A focus on the more energetic GRBs, for example by excluding image triggers (which comprise 17.5 per cent of *Swift* triggers, Lien et al. 2016) and low significance rate triggers, could achieve this.

A byproduct of this selection is that bright GRBs are much more likely to have prompt detections with the UVOT instrument and other optical telescopes, leading to a greater chance of redshift determination and tighter constraints on the model parameters. Among all *Swift* GRBs only 31 per cent have prompt detections with the UVOT instrument, while for the flare sample used here this is 66 per cent.

5.4 Future prospects

Detection of coherent radio emission during the prompt emission phase of a GRB would be a strong indication that a Poynting flux mechanism is preferred over the matter-dominated fireball and other similar models. Detections, or constraining limits, for a small sample of GRBs would allow this result to be generalized and inform further development of prompt emission models.

Work has started to upgrade LOFAR to LOFAR2.0,[2] a significant upgrade that will lead to future improvements for this project. Distinction between the prompt and afterglow phases is important, hence the desire for earlier radio detections. Decreasing the response time may be a realistic prospect for LOFAR2.0. Pushing the LOFAR response time back from 5 to 4.5 min, the number of detectable flares fully within the time window that we predict from our study would increase from 85 to 89, but no further partial flares would be detected. This increases the detected fraction by just 1 per cent, but we acknowledge an increasing incompleteness in the X-ray flare sample at earlier times dependent upon XRT slew time (Section 3). Additionally, one of the key goals of LOFAR2.0 is to significantly enhance the LBA capabilities, leading to more sensitive images in the lowest frequency band and enabling the simultaneous use of the HBA and LBA modes. This will enable us to place tighter constraints at the lower radio frequencies where this emission is expected to peak.

With the recent enhancements to the Murchison Widefield Array (MWA; Tingay et al. 2013) and its significantly faster rapid response mode with slew times as short as 8 s (Hancock et al. 2019), some of the earliest X-ray flares and prompt γ-ray flares may be detectable providing complimentary observations to those obtained by LOFAR (note MWA is less sensitive than LOFAR for longer integrations; Rowlinson & Anderson 2019). Additionally, in the near future, the Square Kilometer Array (SKA; Dewdney et al. 2009)[3] will be built and comprises two facilities: SKA-Mid (350 MHz to 14 GHz) and SKA-Low (50–350 MHz). SKA-Low is expected to provide approximately an order of magnitude improvement in image sensitivity compared to LOFAR and a faster response time, leading to a significantly larger population of radio flares predicted to be observed with the observed γ-ray and X-ray flares.

The launch of the Space Variable Objects Monitor satellite (Wei et al. 2016), planned for launch end 2021, will provide prompt X-ray data down to 4 keV using the ECLAIRS coded mask instrument,

[2] https://www.astron.nl/nl/eu-funded-research/lofar-2-20s
[3] https://www.skatelescope.org

with which ∼70 GRB detections per year are expected. This means that X-ray flares can be picked up at much earlier times, and with GRB localizations in the arcminutes range adequate for immediate LOFAR pointings.

6 CONCLUSIONS

We put forward an observational test of the magnetically dominated wind model of Usov & Katz (2000) as the mechanism for GRB prompt emission. This model predicts low-frequency radio pulses associated with the prompt pulses, which peak at MHz frequencies and may be probed with LOFAR in rapid response mode. We use X-ray flares, shown to arise from sites internal to the jet, to probe GRB prompt emission out to later times, easily accessible with LOFAR. Adopting the *Swift* XRT flare sample compiled by Yi et al. (2016), we apply a magnetically dominated wind model to make predictions for the timing and flux density of corresponding radio pulses. We find that 44 per cent of the flares in this sample would have been detectable with LOFAR HBA at 144 MHz under this model, for typical sensitivities reached using previously executed rapid response mode observations (Rowlinson et al. 2019) and assuming negligible absorption and scattering effects in the interstellar and intergalactic medium. We estimate a rate of order seven *Swift* GRBs per year that would be both accessible to and detected during X-ray flaring by LOFAR. We conclude that such triggered low-frequency radio observations can play a key role in establishing the long debated mechanism, either magnetically or matter dominated, responsible for GRB prompt emission.

ACKNOWLEDGEMENTS

This work was made possible by the ASTRON Helena Kluyver visitor programme enabling RLCS to make an extended visit to AR. RLCS also acknowledges funding from a Science and Technology Facilities Council (STFC) Consolidated Grant to the University of Leicester, and is indebted to L. and K. Wiersema for their support. This work made use of data supplied by the UK Swift Science Data Centre at the University of Leicester. This paper is based (in part) on data obtained with the International LOFAR Telescope (ILT). LOFAR is the Low Frequency Array designed and constructed by ASTRON. The authors thank S. ter Veen for useful discussions and J. Katz for a constructive review.

REFERENCES

Anderson G. E. et al., 2018a, MNRAS, 473, 1512
Anderson M. M. et al., 2018b, ApJ, 864, 22
Balsano R. J. et al., 1998, in Meegan C. A., Koshut T. M., Preece R. D. eds, Proceedings of the Fourth Huntsville gamma-ray burst symposium, Vol. 585, AIPC, p. 428
Band D., Matteson J., Ford L., 1993, ApJ, 413, 281
Bannister K. W., Murphy T., Gaensler B. M., Reynolds J. E., 2012, ApJ, 757, 38
Barthelmy S. et al., 2005, Space Sci. Rev., 120, 143
Bernadini M. G., Margutti R., Chincarini G., Guidorzi C., Mao J., 2011, A&A, 526, 27
Burrows D. N. et al., 2005, Space Sci. Rev., 120, 165
Carbone D., van der Horst A. J., Wijers R. A. M. J., Rowlinson A., 2017, MNRAS, 465, 4106
Chandra P., Frail D. A., 2012, ApJ, 746, 156
Chincarini G. et al., 2007, ApJ, 671, 1903
Chincarini G. et al., 2010, MNRAS, 406, 2113
Cucchiara A. et al., 2011, ApJ, 743, 154
Curran P. A., Starling R. L. C., O'Brien P. T., Godet O., van der Horst A. J., Wijers R. A. M. J., 2008, A&A, 487, 533
Dessenne C. A.-C. et al., 1996, MNRAS, 281, 977
Dewdney P. E., Hall P. J., Schilizzi R. T., Lazio T. J. L. W., 2009, Proc. IEEE, 97, 1482
Evans P. A. et al., 2009, MNRAS, 397, 1177
Evans P. A. et al., 2010, A&A, 519, 102
Evans P. A. et al., 2014, MNRAS, 444, 250
Falcone A. et al., 2007, ApJ, 671, 1921
Gehrels N. et al., 2004, ApJ, 611, 1005
Guidorzi C., Dichiara S., Frontera F., Margutti R., Baldeschi A., Amati L., 2015, ApJ, 801, 57
Guiriec S. et al., 2016, ApJ, 831, L8
Hancock P. J. et al., 2019, PASA, 36, 46
Hu Y.-D., Liang E.-W., Xi S.-Q., Peng F.-K., Lu R.-J., Lü L.-Z., Zhang B., 2014, ApJ, 789, 145
Inoue S., 2004, MNRAS, 348, 999
Ioka K., 2003, ApJ, 598, L79
Jia L.-W., Uhm Z. L., Zhang B., 2016, ApJS, 225, 17
Kaplan D. L., Murphy T., Rowlinson A., Croft S. D., Wayth R. B., Trott C. M., 2016, PASA, 33, e050
Katz J. I., 1994, ApJ, 423, L107
Katz J. I., 1997, ApJ, 490, 633
Levan A. J. et al., 2013, ApJ, 781, 13L
Lien A. et al., 2016, ApJ, 829, 7
Lorimer D. R., Bailes M., McLaughlin M. A., Narkevic D. J., Crawford F., 2007, Science, 318, 777
Margutti R. et al., 2011, MNRAS, 417, 2144
Martin-Carrillo A. et al., 2014, A&A, 567, 84
Meegan C. et al., 2009, ApJ, 702, 791
Oganesyan G., Nava L., Ghirlanda G., Celotti A., 2018, A&A, 616, 138
Rees M. J., Mészáros P., 1994, ApJ, 430, L93
Rees M. J., Mészáros P., 2005, ApJ, 628, 847
Roming P. W. A. et al., 2005, Space Sci. Rev., 120, 95
Rowlinson A., Anderson G. E., 2019, MNRAS, 489, 3316
Rowlinson A. et al., 2019, MNRAS, 490, 3483
Sari R., Piran T., 1999, ApJ, 520, 641
Sari R., Piran T., Narayan R., 1998, ApJ, 497, L17
Sironi L., Petropoulou M., Giannios D., 2015, MNRAS, 450, 183
Smolsky M. V., Usov V. V., 2000, ApJ, 531, 764
Spruit H. C., Daigne F., Drenkhahn G., 2001, A&A, 369, 694
Staley T. D. et al., 2013, MNRAS, 428, 3114
Swenson C. A., Roming P. W. A., 2014, ApJ, 788, 30
Taylor J. H., Cordes J. M., 1993, ApJ, 411, 674
Tingay S. J. et al., 2013, PASA, 30, e007
Troja E., Piro L., Vasileiou V., Omodei N., Burgess J. M., Cutini S., Connaughton V., McEnery J. E., 2015, ApJ, 803, 10
Troja E. et al., 2017, Nature, 547, 425
Uhm Z. L., Zhang B., 2016a, ApJ, 824, L16
Uhm Z. L., Zhang B., 2016b, ApJ, 825, 97
Usov V. V., Katz J. I., 2000, A&A, 364, 655
Van Haarlem M. P. et al., 2013, A&A, 556, 2
Vestrand W. T. et al., 2014, Science, 343, 38
Wang F. Y., Dai Z. G., 2013, Nat. Phys., 9, 465
Wei J. et al., 2016, "The Deep and Transient Universe: New Challenges and Opportunities - Scientific prospects of the SVOM mission," Proceedings of the Workshop, preprint (arXiv:1610.06892)
Yi S.-X., Xi S.-Q., Yu H., Wang F. Y., Mu H.-J., Lü L.-Z., Liang E.-W., 2016, ApJS, 224, 20
Zheng W. et al., 2012, ApJ, 751, 90

This paper has been typeset from a TEX/LATEX file prepared by the author.